

# Nonlinear MHD Simulation of Pressure Deformation Dynamics in the Large Helical Device

MIURA Hideaki, HAYASHI Takaya and SATO Tetsuya  
*National Institute for Fusion Science, Toki 509-5292, Japan*

(Received: 11 December 2001 / Accepted: 17 May 2002)

## Abstract

Nonlinear behaviors of a magnetohydrodynamic (MHD) plasma in the Large Helical Device (LHD) are investigated by means of a numerical simulation. Computations for a configuration with the radius of the vacuum magnetic axis  $R_{ax} = 3.6$  m are conducted under the stellarator symmetry. The MHD plasma is observed to be dominated by a ballooning instability. Simulations with several cases of resistivities show that the saturation levels of the plasma kinetic energy are nearly proportional to the resistivity. The numerical results are compared with our previous simulation results on  $R_{ax} = 3.7$  m. The saturation levels are found to be almost comparable between the two configurations, although the  $R_{ax} = 3.7$  m configuration is more magnetically hilly and Mercier-unstable. Pressure budget analysis shows that viscous heating plays a key role in making pressure deformations saturated.

## Keywords:

nonlinear MHD simulation, pressure deformation, viscous heating

## 1. Introduction

Understanding of complex nonlinear behaviors of an MHD plasma is important for achievement of successful confinement of plasmas in fusion devices. Numerical simulation is one of the most powerful and successful approaches to investigate the subject. Though huge memory and long computational time are necessary for a nonlinear simulation on a helical device with fully three-dimensional (3D) geometry, recent development of high-performance supercomputers has enabled us to conduct such a large computation. Recently, we have developed a numerical code to simulate full 3D, compressible and dissipative MHD equations in a helical device [1]. Our previous simulations on a LHD configuration with the magnetic axis at  $R_{ax} = 3.7$  m [2], under the stellarator symmetry, has shown excitation of unstable modes, which are dominated by the resistive ballooning instability, and saturation of the excited modes.

In this paper, we aim to investigate full 3D nonlinear behaviors of an MHD plasma in the LHD with the magnetic axis at  $R_{ax} = 3.6$  m and compare with the results of the previous simulations with  $R_{ax} = 3.7$  m. While it is known that at LHD configuration becomes more magnetically hilly and Mercier-unstable as the magnetic axis is shifted inwardly [3], a series of experiments with  $R_{ax} = 3.6$  m reports a better confinement than a  $R_{ax} = 3.7$  m configuration [4]. We expect that a comparison of  $R_{ax} = 3.6$  m and 3.7 m simulations allows us to investigate why and how a good confinement is achieved with  $R_{ax} = 3.6$  m magnetic axis from a viewpoint of nonlinear MHD.

In Sec. 2, the outline of our simulations is described. In Sec. 3, numerical results by our nonlinear simulations are shown. We investigate growth of the kinetic energy as an indicator of plasma fluctuation. We pay also our special attention to pressure deformation

---

Corresponding author's e-mail: [miura@toki.theory.nifs.ac.jp](mailto:miura@toki.theory.nifs.ac.jp)

because the pressure gradient should be the main source to drive an instability in the system studied in this paper. Summary is shown in Sec. 4.

## 2. Outlines of Simulations

We solve the fully-nonlinear, compressible and resistive MHD equations in a full 3D geometry. The stellarator symmetry is imposed in the toroidal direction. We set the position of the vacuum magnetic axis to be  $R_{ax} = 3.6$  m. In our numerical code, we adopt 4th-order accuracy discretization schemes both in time and space. Number of grid points are  $97 \times 97$  on a poloidal section and 32 in the toroidal direction for a half-pitch period. Refer to ref. 2 on details of our simulation code. (See also ref. 5 on normalization of the MHD equations.)

In Fig. 1, profiles of an initial ideal equilibrium are shown. This equilibrium is obtained by the use of the HINT code [5]. An initial pressure profile is given by  $p(\psi) = p(0) (1 - \psi)^2$  where  $\psi$  is the initial normalized

toroidal flux. Figures 1(a) and 1(b) are the Poincaré plots of magnetic lines on horizontally- and vertically-elongated poloidal section, respectively. The outer side of the torus is in the right-hand side. The profile of the rotational transform,  $\iota$ , is shown in Fig. 1(c) as a function of the mean plasma radius. From the calculation of the specific volume, the core part of the configuration has a property of magnetic well while the edge region is magnetic hill. In Figs. 1(d) and 1(e), bird's eyes views of the pressure and the toroidal current on a poloidal section  $\phi = \pi/20$  ( $\phi$  is the toroidal angle) are shown, respectively. The central beta,  $\beta_0$ , is about 3.6 %. Note that an initial equilibrium which is used in ref. 2 is roughly described by  $R_{ax} = 3.7$  m, the initial pressure profile being  $p(\psi) = p(0) (1 - \psi)^2$  and  $\beta_0 = 4$  %. Thus differences in the results of two series of simulations compared in the next section are mainly brought about by the difference in  $R_{ax}$  for the initial equilibria.

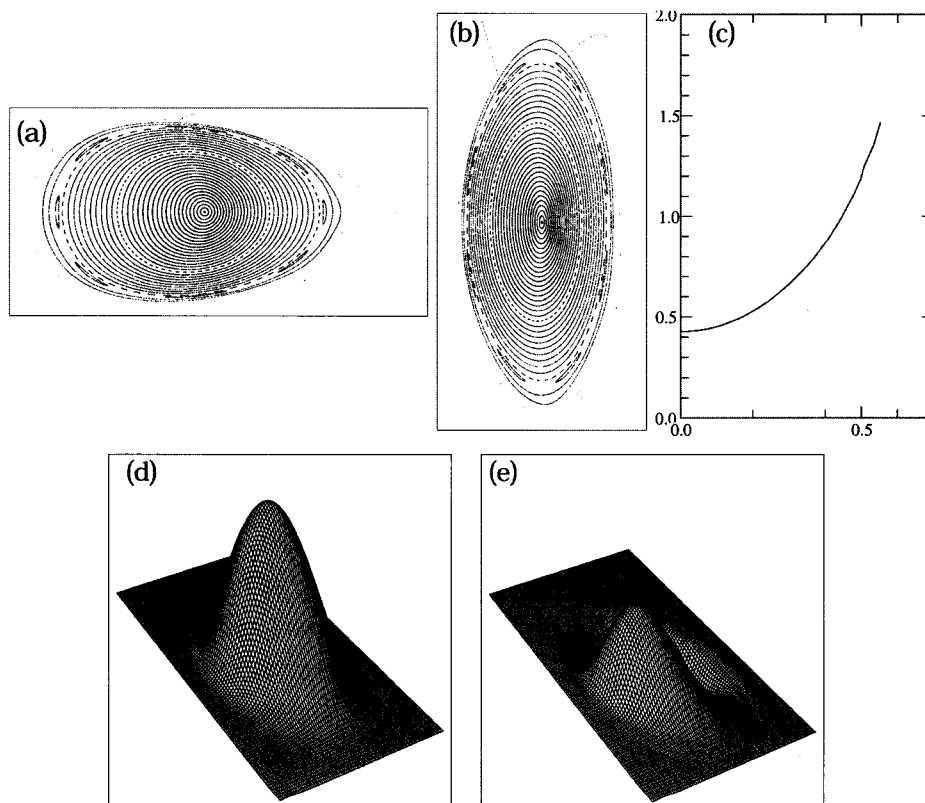


Fig. 1 An initial equilibrium computed by the HINT code. The Poincaré plot of the magnetic field lines on (a) the horizontally-elongated poloidal section, (b) the vertically-elongated poloidal section. The outer side of the torus is in the right-hand side. (c) The rotational transform plot. The abscissa is the mean plasma radius. Bird's eyes views of (d) the pressure and (e) toroidal current on  $\phi = \pi/20$  poloidal section.

### 3. Nonlinear Simulations and Pressure Deformations

In this section, we see numerical results of our nonlinear full 3D simulations. In the MHD equations, there are three intrinsic parameters: the conductivity  $\kappa$ , resistivity  $\eta$  and viscosity  $\mu$ . In this paper, we fix  $\kappa = 1 \times 10^{-6}$  and  $\mu = 2 \times 10^{-3}$  throughout this article and study the influence of the resistivity by varying  $\eta$  from  $1 \times 10^{-6}$  to  $1 \times 10^{-5}$ .

In Fig. 2, we see time evolution of the averaged kinetic energy per unit density  $E_K = 1/2 \langle v_i v_i \rangle$  ( $v_i$  is the  $i$ -th component of the velocity vector and  $\langle \cdot \rangle$  represents the volume average) for five values of the resistivity  $\eta = 1 \times 10^{-6}$ ,  $10^{1/4} \times 10^{-6}$ ,  $10^{1/2} \times 10^{-6}$ ,  $10^{3/4} \times 10^{-6}$  and  $1 \times 10^{-5}$ . It is observed that  $E_K$  grows almost exponentially first, and begins to decay gradually for all of the five resistivities. We shall see later that the exponential growth in Fig. 2 is dominated by the ballooning instability.

In Fig. 3(a), saturation levels  $\sigma$  of the kinetic energy growth are plotted as a function of the resistivity  $\eta$ . Here we define the saturation level as the maximum value of the kinetic energy. A least-square fitting shows  $\sigma \propto \eta^{0.9}$ . Thus  $\sigma$  is almost proportional to  $\eta$ . In Fig. 3(b), time evolutions of  $E_K$  with  $R_{ax} = 3.6$  m (solid line) and 3.7 m (dashed line) are shown. The resistivity is  $\eta = 10^{1/2} \times 10^{-6}$  for both of the two simulations. We find that  $E_K$  of the  $R_{ax} = 3.6$  m simulation grows faster than that of the  $R_{ax} = 3.7$  m simulation. It is a direct result of the former configuration being more Mercier-unstable than the latter. Note that the two kinetic energies saturate at almost the same level despite the difference of the growth rates. We checked the levels of  $\sigma$  for three values of resistivity  $\eta = 1 \times 10^{-6}$ ,  $10^{1/4} \times 10^{-6}$ , and  $10^{1/2} \times 10^{-6}$  of  $R_{ax} = 3.7$  m simulations and verified that  $\sigma$  of  $R_{ax} = 3.7$  m simulations are comparable with those of  $R_{ax} = 3.6$  m simulations. Furthermore, as we shall see in the next paragraph, an instability observed in this article is not destructive and a plasma confinement is recovered in the latter stage of the simulations. These two facts suggest that the saturation level of an instability is not sensitive to a detailed value of  $R_{ax}$ , because of a nonlinear property of an MHD plasma.

In Figs. 4(a) and (b), contour plots of the pressure on horizontally- and vertically-elongated poloidal sections at  $t = 1400 \tau_A$  ( $\tau_A$  is the Alfvén time unit), obtained by a simulation with  $\eta = 10^{1/2} \times 10^{-6}$ , are shown, respectively. The outer side of the torus is in the right-hand side. Contours are deformed in the course of the time evolution at around  $\iota = 2/3$  region where the

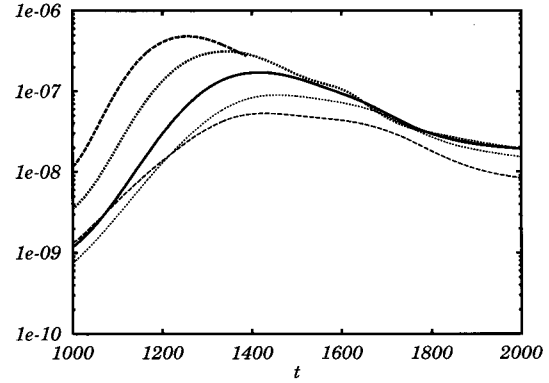


Fig. 2 Time evolution of the averaged kinetic energy. Thick dashed, thick dotted, thick solid, thin dotted, thin dashed lines represent simulations with  $\eta = 1 \times 10^{-6}$ ,  $10^{1/4} \times 10^{-6}$ ,  $10^{1/2} \times 10^{-6}$  and  $10^{3/4} \times 10^{-6}$ , and  $1 \times 10^{-5}$ , respectively.

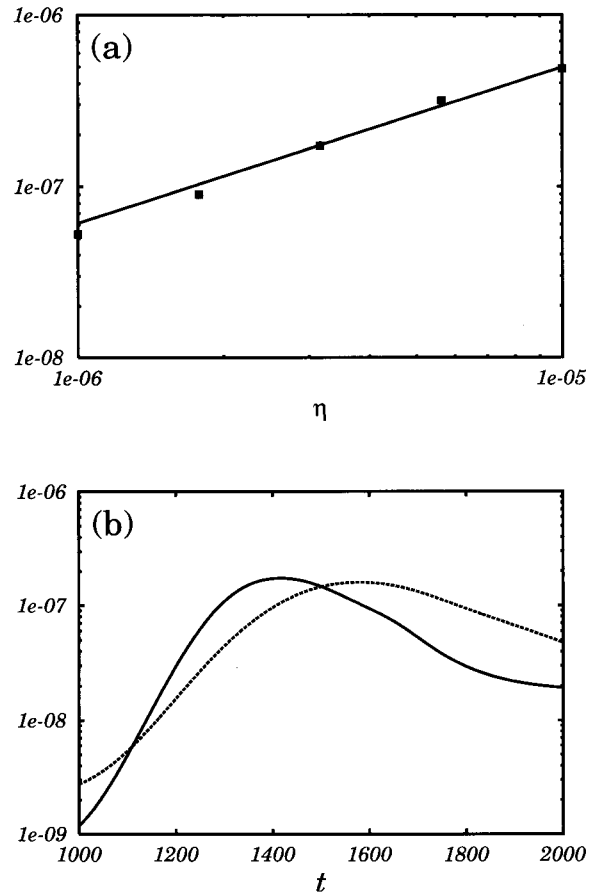


Fig. 3 (a) Saturation level  $\sigma$  as a function of the resistivity  $\eta$ . Solid line represents  $\sigma \propto \eta^{0.9}$ . (b) A comparison of the kinetic energy growth between  $R_{ax} = 3.6$  m and  $R_{ax} = 3.7$  m simulations. Solid and dashed lines represent  $R_{ax} = 3.6$  m and  $R_{ax} = 3.7$  m simulations, respectively.

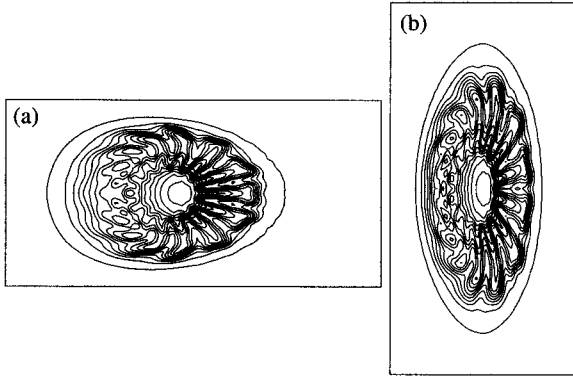


Fig. 4 Contour plots of the pressure on horizontally- and vertically-elongated poloidal sections. Outer side of the torus is in the right-hand side to the paper. The time stamp is  $t = 1200 \tau_A$  in (a) and (b).

pressure gradient is the steepest, especially in the outer side of the torus. Poloidal and toroidal Fourier mode numbers are estimated to be 15 and 10, respectively. Furthermore, pressure deformations are clearer on the horizontally-elongated poloidal section than the vertically-elongated poloidal section. An analysis which is similar to that seen in Miura *et al.* [2] reveals that the pressure deformations are dominated by the resistive ballooning instability. It is also observed that plasma confinement, for which the pressure profile becomes broader, is recovered after a sufficiently long time development.

Next, in order to clarify a physical mechanism which drives or suppresses pressure deformations observed in Fig. 4, we calculate volume integrals of the rhs. terms of the pressure-budget equation as has been done in ref. 2. In Fig. 5(a), the pressure flux, compression, conduction, ohmic heating and viscous heating terms are shown for the period  $1000 \tau_A \leq t \leq 2000 \tau_A$ . It is clear that the viscous heating term (a dashed line) dominates the pressure budget. Next, the five terms are integrated for positive and negative values separately and plotted in Fig. 5(b). It is clear that the pressure flux term has the largest amplitude. It is consistent with a result shown in Ref. 2, in which it is shown that the pressure flux is a profile in phase with the pressure fluctuation and drives pressure deformations. Note that the viscous heating term grows rapidly just before  $t \approx 1400 \tau_A$ , when the kinetic energy becomes maximum. A rapid growth just before the nonlinear saturation suggests that the viscous heating term plays a crucial role in the saturation.

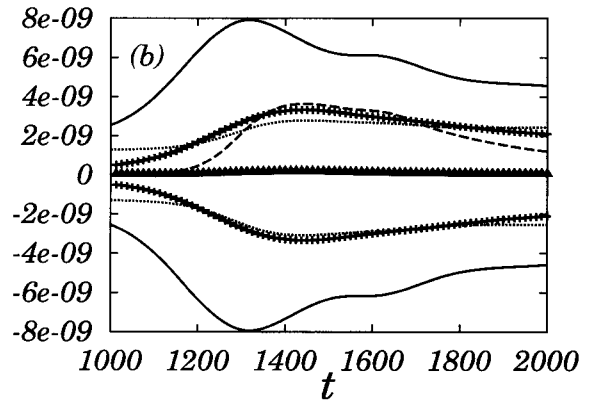
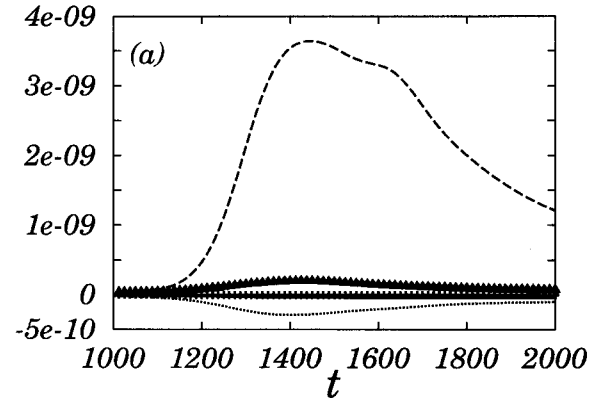


Fig. 5 Pressure budget evaluation for a  $\eta = 10^{12} \times 10^{-6}$  simulation. The pressure flux, compression, thermal conduction, ohmic heating and viscous heating terms are represented by solid line, dotted line, dashed line, cross and triangles, respectively. (a) Volume integration of the five terms in the right-hand side of the pressure budget equation over the system. (b) Volume integration of the five terms for their positive and negative value regions.

#### 4. Concluding Remarks

We have conducted a series of nonlinear MHD simulations on the LHD system with the position of the magnetic axis  $R_{ax} = 3.6$  m. Our simulations have shown that the saturation level of the kinetic energy is nearly proportional to  $\eta$ :  $\sigma \propto \eta^{0.9}$ . It implies that the saturation level becomes sufficiently small when the resistivity tends to a small value available in the LHD experiments, suggesting that an instability observed in the experiments can be quite mild. Although paying too much attention to the precise value of the scaling exponent 0.9 does not make sense because the number of samples are small and range of  $\eta$  is too short (one decade), it still seems that the scaling exponent 0.9

is much greater than a value expected from a growth rate of the resistive ballooning instability  $1/3$ . It suggests that, in order to explain the behaviors of  $\sigma$ , the nonlinearity of the MHD equations (the viscous heating effect, for example) should be taken into account. It is worth emphasizing here again that the saturation levels in the  $R_{ax} = 3.6$  m simulations are almost comparable with  $R_{ax} = 3.7$  m cases. So far as a system under the stellarator symmetry is concerned, these two facts suggest that a plasma can be confined even with a small (shifted to inward)  $R_{ax}$  because of the nonlinear property of a plasma.

This simulation research was conducted by making

use of the supercomputer NEC SX-4/64M2 in the theory and computer simulation center of NIFS.

### References

- [1] H. Miura *et al.*, to be published in J. Plasma Fusion Res. SERIES 4.
- [2] H. Miura *et al.*, Phys. Plasmas **8**, 4870 (2001).
- [3] Ichiguchi *et al.*, Nucl. Fusion **33**, 481 (1993).
- [4] N. Ohyabu *et al.*, Phys. Rev. Lett. **84**, 103 (1999).
- [5] T. Hayashi, A. Takei and T. Sato, Phys. Fluids B **4**, 1539 (1992); Harafuji *et al.*, J. Comput. Phys. **81**, 169 (1989).